DESIGN AND OPTIMIZATION OF ELECTROSTATIC DEFLECTORS FOR ELENA

D. Barna, University of Tokyo, Japan
W. Bartmann, M. Fraser, R. Ostojic, CERN, Switzerland

Abstract

The ELENA ring [1] will decelerate the antiprotons ejected from the Antiproton Decelerator (AD) at 5.3 MeV down to 100 keV kinetic energy. The slow antiprotons will be delivered to experiments using electrostatic beamlines, consisting of quadrupoles, correctors and deflectors. An extensive simulation study was carried out to find solutions to minimize the aberrations of the deflectors. These solutions will be presented together with the actual design of these devices.

INTRODUCTION

At low particle energies electrostatic devices have many advantages over magnetic ones, for example the absence of remanent magnetic fields, no need for cooling, cheap and simple production. Following a cost-performance analysis, electrostatic beamlines were chosen for ELENA.
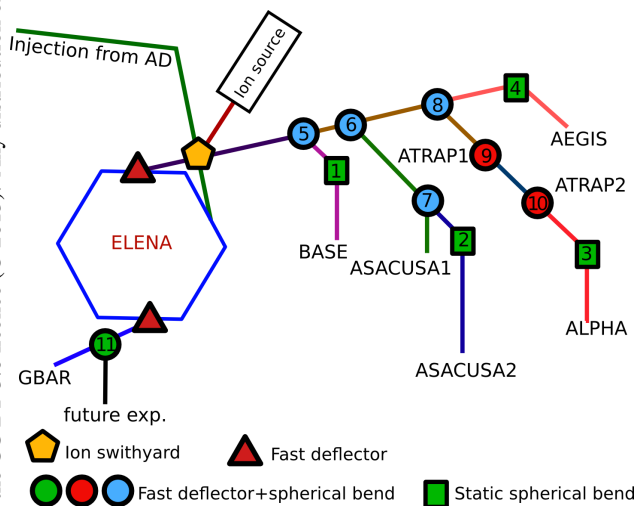

Figure 1: Layout of the ELENA transfer lines.

The schematic layout of the ELENA transfer lines is shown in Fig. 1. Due to the constraints given by the existing experiments and other equipment already present in the AD hall, the angles of the different bends could not be made equal. However, they can be arranged into groups with nearly equal angles. In order to facilitate the design, manufacturing and spare part management, identical electrode structures will be used at these positions with slightly different voltage settings to account for the different bending angles. In most cases the deflectors will have custom vacuum chambers to match the actual angle of the beamline. The deflectors of the ELENA transfer lines can be grouped into following types (Table 1):

1. Fast switch (FS) combinations: ELENA will deliver 4 antiproton bunches with a spacing of about 1 µs in a single extraction. These bunches will be distributed among 4 experiments running simultaneously using fast switches in the beamlines. This functionality is realized by a combination of a fast electrostatic deflector [2] (the same device which is used for ejection from the ring) and a static deflector. The fast deflector has a rise time <1 µs and gives an initial kick of 220 mrad. The static deflector gives the remaining deflection. The fast switches can be further classified into two groups:

   (a) Horizontal fast switches (HFS at positions 5, 6, 7, 8 and 11 in Fig. 1) - these devices deflect the beam in the horizontal plane by a total angle between 45.7° and 48.1°.

   (b) Vertical fast switches (VFS at positions 9 and 10 in Fig. 1) - these devices deflect the beam vertically to ATRAP1 and ATRAP2.

2. Standalone static deflectors will deflect the beam by an angle between 45.77° and 50.42° at positions 1, 2, 3 and 4 in Fig. 1.

Table 1: List of Electrostatic Deflectors

Pos. in Fig. 1	Tot. defl. [deg]	Type	Electrode angle [deg]	Range [deg]
1,2	48.1	Static		
3	50.42	Static	48	±2.3
4	45.77	Static		
5,6,7	48.08	HFS	34.3	±1.2
8	45.76	HFS		
9,10	90	VFS	77.4	0
11	t.b.d.	HFS	t.b.d.	0

OPTIMIZATION OF ELECTRODES

The mechanical aperture (A in Fig. 2a) was chosen to be 65 mm - slightly larger than the value adopted for the beamlines in general (60 mm) due to the following reasons: the fringe field of the device deflects the particles already outside of the electrodes, and the central particle trajectory deviates from the nominal arc towards the bending center. Also, the same device will be used for slightly different bending angles, which gives a further excursion of the central particle trajectory from the nominal arc. A larger aperture

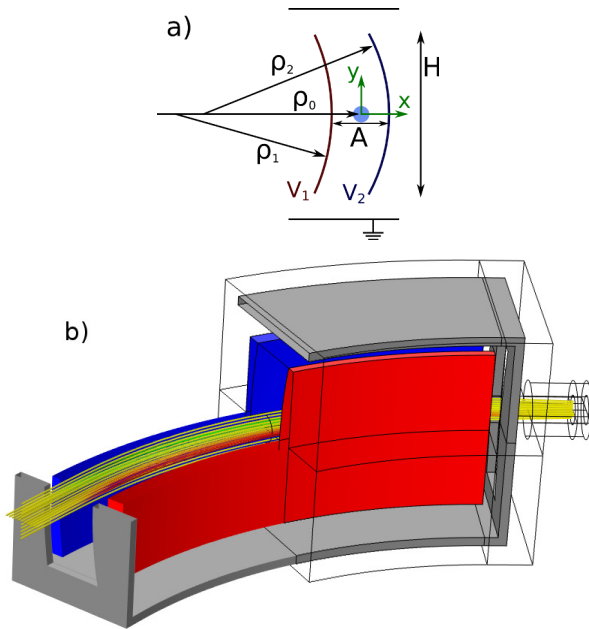also relaxes the required mechanical tolerances of the electrodes.

Figure 2: a) Cross-section of the deflector in the non-bending plane. b) The COMSOL model with the simulated particles. Color indicates kinetic energy.

The electric field needed to keep charged particles on a circular orbit scales inversely with the orbit radius ρ_0. Aberrations also decrease with larger bending radius. A value of ρ_0=600 mm was chosen as a best compromise to keep the size of the device within the required limits. The required voltages of the electrodes are approximately $\pm AE_{kin}/q\rho_0 = \pm 10.8$ kV.

The radius of curvature of the electrodes in the non-bending plane (ρ_1 and ρ_2) and their height H are free parameters (Fig. 2a). The height of the electrodes was chosen to be $H = 180$ mm as it can be introduced into the vacuum chamber through a DN200CF flange.

The radii of curvature of the electrodes ρ_1 and ρ_2 affect the optical properties of the deflector: the focusing strengths in the two planes and the aberrations. The dominant aberrations of an electrostatic deflector of this type are $\delta x'_{out} \sim x^2$, $\delta x'_{out} \sim y^2$ and $\delta y'_{out} \sim xy$ where x_{out} and y_{out} are the transverse coordinates and x'_{out} and y'_{out} are the trajectory derivatives at the output. It can be shown that the minimization of the last two of these give the same constraints on the electrode radii.

A set of particles with input coordinates (-20 mm $< x_{in} < 20$ mm, $x'_{in} = 0, y_{in} = 0, y'_{in} = 0$) and ($x_{in} = 0, x'_{in} = 0, -20$ mm $< y_{in} < 20$ mm, $y'_{in} = 0$) was traced through the 3D fieldmap (Fig. 2b) of the standalone or combined devices with different radii of curvature of the electrodes ρ_1 and ρ_2. The output phase-space profiles of these beams were fitted with $x'_{out} = c_x^{(1)} x_{out} + c_x^{(2)} x_{out}^2 + c_x^{(3)} x_{out}^3$ and $x'_{out} = c_y^{(2)} y_{out}^2$ (due to the symmetry of the device only even powers of y_{out} appear).

5: Beam Dynamics and EM Fields

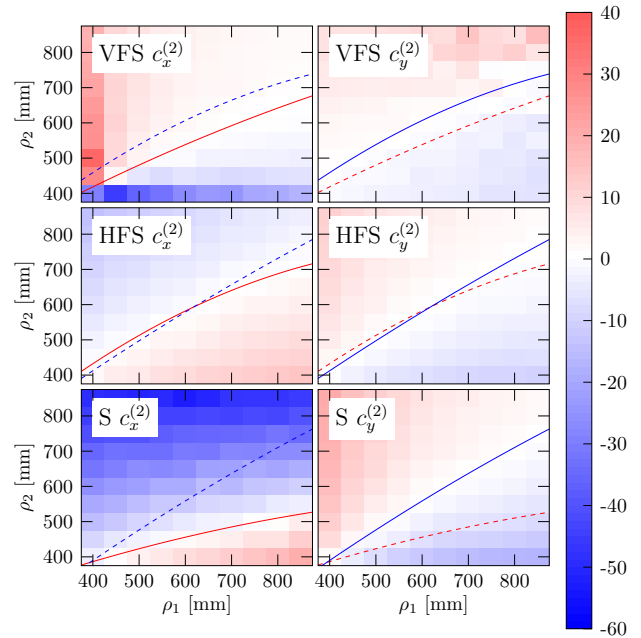**D01 - Beam Optics - Lattices, Correction Schemes, Transport**

Figure 3: The 2nd order aberration coefficients as a function of radius of curvature of the electrodes ρ_1 and ρ_2 for the standalone (S), horizontal and vertical fast switch (HFS, VFS) variants with bending radius $\rho_0 = 600$ mm. The solid lines indicate the minimum of the given plot; the dashed lines indicate the minimum in the other plane.
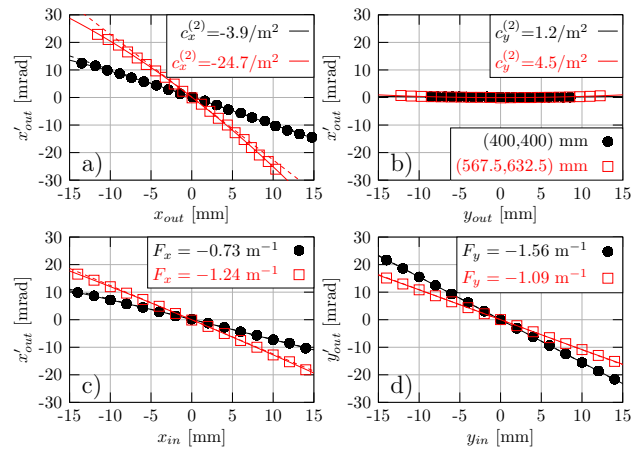

Figure 4: a) b) Visualization of the $\delta x'_{out} \sim x^2$ and $\delta x'_{out} \sim y^2$ aberrations of the standalone deflector for two geometries (black circles: optimized geometry; red squares: spherical deflector) The solid lines are the fitted polynomials (see text), the dashed lines are the linear terms. c) d) Focusing powers (slope of the $x'_{out} - x_{in}$ and $y'_{out} - y_{in}$ curves).

The 2nd order coefficients $c_x^{(2)}$ and $c_y^{(2)}$ are shown in Fig. 3 as a function of ρ_1 and ρ_2 for the three different types of deflectors with the minimum-aberration lines overlaid.

For the standalone deflector $\rho_1 \sim \rho_2 \sim 400$ mm have been chosen to minimize $\delta x'_{out} \sim x^2$ and $\delta x'_{out} \sim y^2$ aberrations simultaneously. Figs. 4 a) b) demonstrate the improved linearity of this device with the optimal geometry $\rho_1 =$
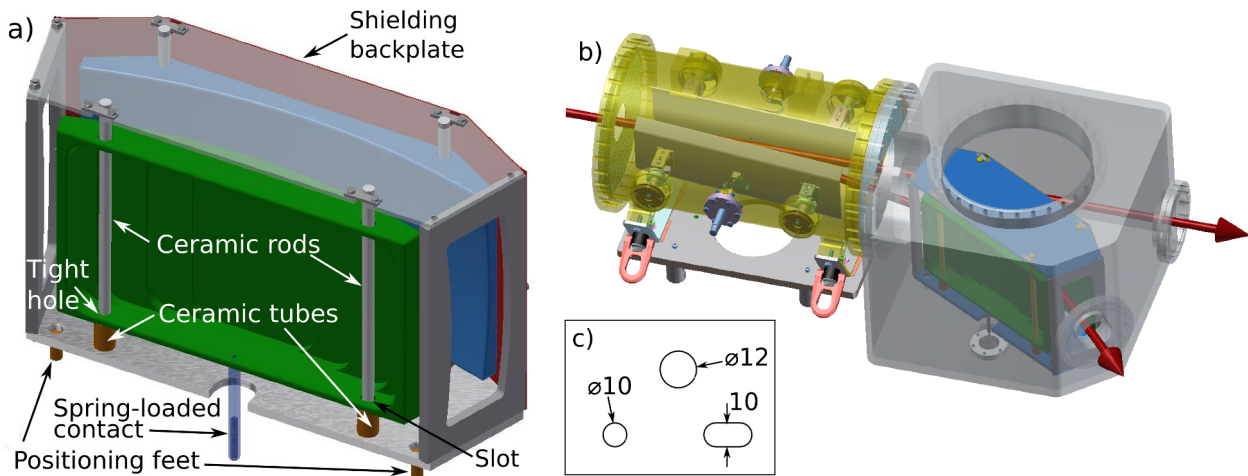
Figure 5: a) The mechanical design of the electrode structure of the horizontal static deflectors (standalone or quick switch combination). b) The horizontal fast-switch combination. c) Schematics of the alignment holes in the bottom plate of the vacuum chamber.

$\rho_2 = 400$ mm compared to a spherical deflector with $\rho_1 = 567.5$ mm, $\rho_2 = 632.5$ mm. The shape of the electrodes affects the focusing powers of the deflector (Fig. 4 c) d). In contrast to the spherical deflector which is known to have nearly equal focusing powers in the two planes (red lines), the optimized device focuses in the non-bending plane twice as strongly as in the bending plane (black lines).

For the combined deflectors HFS and VFS the intersection (or point of closest approach) of the two lines is not well defined, one can choose different geometries. Minimum aberrations and nearly equal focusing power in the two planes are obtained for $\rho_1 = \rho_2 = 550$ mm (not shown).

A full beamline simulation study (where individual particles were traced through the 3D fieldmaps of all devices of the longest beamline) has shown that the accumulated effect of nonlinearities of the electrostatic devices is negligible at the experimental handover points [3].

MECHANICAL DESIGN

The two electrodes will be mounted in a grounded frame as a separate unit, as shown in Fig. 5a. Each electrode is supported by two ceramic rods and tubes. One of the rods is fitted into a tight hole of the electrode; the other rod is going through a slotted hole. This solution allows an eventual different thermal expansion of the electrodes and the frame during bake-out at 250 °C in both horizontal and vertical directions, without compromising the alignment precision of the electrodes. In case of the quick switch combinations an electrical shielding plate will be mounted to the electrode assembly in order to shield the non-deflected beam from the electrical field of the electrodes.

This electrode frame will be placed in a vacuum chamber as shown in Fig. 5b for the horizontal quick switch combination, relying on gravity for mounting. The three feet of the frame (two of which are visible in Fig. 5a) will be positioned in three alignment holes machined into the bottom plate of

the vacuum chamber as shown schematically in Fig. 5c. One of these holes is fitting the frame foot tightly; the slotted hole allows movement in one direction thereby allowing a different thermal expansion of the frame compared to the vacuum chamber. The third hole allows movement in the horizontal plane.

The electrical connections use spring-loaded contacts and commercial SHV-20 kV feedthroughs on the bottom of the vacuum chamber.

CONCLUSIONS

The electrostatic deflectors of the ELENA beamlines have been optimized so that the second order aberrations are effectively eliminated. For the standalone deflector the optimal electrode radii are $\rho_1 = \rho_2 = 400$ mm giving twice as strong focusing in the non-bending plane as in the bending plane. For the fast+static deflector combinations the aberrations could be minimized with different geometries; for the chosen radii of $\rho_1 = \rho_2 = 550$ mm the focusing powers of the device in the two transverse planes are equal. Full beamline simulations have shown that the effects of the nonlinearities of the deflectors and other electrostatic elements are negligible. The mechanical design of the deflectors is in an advanced state.

REFERENCES

[1] V. Chohan (editor) et al., "Extra Low ENergy Antiproton (ELENA) ring and its Transfer Lines: Design Report", http://cds.cern.ch/record/1694484

[2] J. Borburgh et al, "Concept for ELENA Extraction and Beam Transfer Elements", MOPFI061, Proceedings of IPAC'13, Shanghai, China.

[3] M. Fraser, "Beam Dynamics Studies of the ELENA Electrostatic Transfer Lines", MOPJE044, *These Proceedings*, IPAC'15, Richmond, USA.